Applied Environmental Research (2026) 48(1), 006
https://doi.org/10.35762/AER.2026006

Applied Environmental Research
- RESEARCH FOR SUSTAINABLE PLANET -

Research Article

Activated Carbon Prepared from Residual Eucalyptus Wood for the Removal of Methyl Orange: Equilibrium, Kinetics, Thermodynamics, and Desorption

Mathin Jaikua[1], Phuthidhorn Thana[2], Sunisa Ungwiwatkul[3], Jakkrawut Maitip[3], Kanyarak Prasertboonyai[3,*]

[1] *Energy Technology and Management Program, Faculty of Science, Energy and Environment, King Mongkut's University of Technology North Bangkok (Rayong Campus), Rayong 21120, Thailand*
[2] *Data Science and Computation Program, Faculty of Science, Energy and Environment, King Mongkut's University of Technology North Bangkok (Rayong Campus), Rayong 21120, Thailand*
[3] *Chemical Industrial Process and Environment Program, Faculty of Science, Energy and Environment, King Mongkut's University of Technology North Bangkok (Rayong Campus), Rayong 21120, Thailand*

*Corresponding Email: kanyarak.p@sciee.kmutnb.ac.th

Abstract

This research utilizes activated carbon derived from residual Eucalyptus wood (EW) for the removal of methyl orange (MO). The residual Eucalyptus wood-based activated carbon (EWAC) was produced through carbonization at 400 °C (EWC) followed by activation with a mass ratio of H_3PO_4 to EWC of 1:3, which was conducted at 800 °C for 1 h. The characterization of the EWAC involved various analytical techniques, including FTIR, XRD, BET, and CHN analysis. The adsorption parameters, such as pH (range: 3–8), adsorbent dose (range: 0.01–0.5 g per 50 mL of MO solution), contact time (range: 5–720 min), initial MO concentration (range: 5–600 mg L^{-1}), and temperature (range: 20–40 °C), were investigated. The kinetic study suggested that the adsorption behavior correlated well with the pseudo-second-order model, indicating a suitable fit for the experimental data. The intraparticle diffusion analysis suggested that the external film diffusion of dye molecules controls the overall adsorption rate. Moreover, the adsorption model provided good fit with the Langmuir isotherm model, confirming monolayer adsorption with an adsorption capacity (q_{max}) of 29.11 mg g^{-1} at 303.15 K. Thermodynamic studies also confirmed that endothermic and chemisorption processes are favored for the adsorption process even at high temperatures. Furthermore, the EWAC demonstrated potential for regeneration and reuse over four operational cycles, highlighting its cost-effectiveness and eco-friendly nature for removing MO from synthetic dyes in wastewater.

ARTICLE HISTORY

Received: 23 Oct. 2025
Revised: 22 Jan. 2026
Accepted: 2 Feb. 2026
Published: 5 Feb. 2026

KEYWORDS

Eucalyptus wood;
Adsorption;
Activated carbon;
Methyl orange;
Dye removal

Introduction

Effluents that contain dyes are commonly used in a variety of industries, such as textiles, paint, paper, plastic, cosmetics, and food processing. Unfortunately, these dyes have complex chemical structures with various toxic, carcinogenic, mutagenic, and allergenic properties (Rahmani et al., 2013). If these untreated dyes accumulate in water sources, they can negatively impact both human health and the environment. Additionally, untreated dyes are highly stable and resistant to chemical, photochemical, and biological breakdowns (Islam et al., 2017). As a result, adequate disposal of such dyes is critical to have a beneficial impact on living beings and the environment.

Some of the several techniques for removing dyes include advanced oxidation processes, coagulation–flocculation, photocatalytic degradation, ozonation, and ion exchange (Pornsawai et al., 2022). However, these

technologies have several disadvantages, including exorbitant costs, a large volume of hazardous sludge formation and disposal, partial removal, high energy consumption, and the use of excessive chemicals. As a result, there is a need to remove dyes from wastewater and develop a treatment technology that is simple, successful, and cost-effective (Kittappa et al., 2020). Adsorption remains one technique for removing color from wastewater that has proven to be more popular, cost-effective, and efficient because of its simplicity, reliability, low cost, ease of operation, and ease of recovery of the adsorbent compared to the other conventional treatment methods (Sawasdee et al., 2024; Khamdahsag et al., 2021).

In recent years, activated carbon (AC) has become the most popular and simplest adsorbent for dye adsorption because of its vast surface area, high adsorption capacity, and various functional groups (Islam et al., 2017). Furthermore, producing AC from low-cost, renewable precursors such as biomass waste has proven to be a fascinating study topic (Chen et al., 2013). Previous studies have reported that agricultural wastes have been widely utilized as precursors for biomass-based adsorbents owing to their high carbon content, low ash composition, abundant active sites, and large specific surface area (Bella et al., 2022), such as spent tea leaves (Fatama et al., 2024) [9], coconut shells (Ipeaiyeda et al., 2020), palm kernel shells (Ipeaiyeda et al., 2020), coffee (Chiang et al., 2020), pineapple waste (Pasukphun and Suma, 2017), tamarind wood (Phothi-tontimongkol and Prasertboonyai, 2024) and rice husk (Menya et al., 2018).

Eucalyptus wood has become an interesting source of biochar feedstock because of its high productivity (more than 58 mt per hectare per year) and its ability to renew and overgrow (Rockwood et al., 2019). In addition, Eucalyptus wood charcoal has already been suggested for the adsorption of many pollutants, such as arsenic (Fuentes et al., 2021), lead (Singh et al., 2023), natural aluminum dye (Saowanee and Tangsathitkulchai, 2013), crystal violet (Singh et al., 2018), methylene blue (Han et al., 2020) and malachite green dye (Singh et al., 2016).

The AC is produced via the gradual pyrolysis of lingocellulosic biomass, in which carbon-rich precursors are heated to form a porous carbon structure. This process can involve two main activation methods: physical acti-vation, which requires high temperatures, and chemical activation, which occurs at lower temperatures using reagents such as $ZnCl_2$, KOH, NaOH, and H_3PO_4 to enhance porosity and surface characteristics (Ncibi et al., 2014; Brito et al., 2018). Among these reagents, H_3PO_4 offers several advantages—including lower activation temperatures, higher carbon yields, and the development of predominantly mesoporous structures (Phothitontimongkol and Prasertboonyai, 2022). Moreover, the lower activation temperature enables the retention of acidic functional groups (e.g., carboxyl and phenolic hydroxyl groups) and the introduction of phosphorus species, thereby increasing the dye adsorption capability (Kazmierczak-Razna et al., 2017; Luo et al., 2019; Pereira et al., 2003). Compared with their untreated counterparts, chemically activated adsorbents routinely exhibit greater surface areas and adsorption capacities, which drives a growing demand for cost-effective AC derived from various biomass resources.

Therefore, this study aims to synthesize AC derived from eucalyptus wood through a two-step process consisting of carbonization and chemical activation via phosphoric acid (H_3PO_4). The prepared adsorbent was applied for the removal of methyl orange (MO), which serves as a model dye to evaluate the influence of key operating parameters and to elucidate the adsorption behavior. In addition, the adsorption isotherms, kinetics, and mechanisms were systematically analyzed to better understand the interaction between MO molecules and eucalyptus wood-based activated carbon (EWAC). The reusability of EWAC was also examined to assess its potential for sustainable wastewater treatment applications.

Materials and methods

1) Materials and reagents

All of the chemicals employed in this study were of analytical reagent grade. MO (formula wt. $C_{14}H_{14}N_3NaO_3S$ and molecular wt. 327.34), hydrochloric acid (HCl), and sodium hydroxide (NaOH) were purchased from Sigma Aldrich. Phosphoric acid (85% H_3PO_4, Ajax Finechem Pty) was used for chemical activation.

2) Preparation of adsorbents

The residual eucalyptus wood biomass, locally sourced from Rayong Province, Thailand, was used as the raw material for this study. The collected eucalyptus wood was first coarsely cut via a cutting mill and subsequently sun-dried to remove moisture. The dried biomass was then subjected to carbonization at 400 °C for 1 h to produce eucalyptus wood biochar (EWC). The resulting carbon was crushed, sieved to obtain a uniform particle size, and stored in airtight containers until further use.

To prepare the EWAC, the precarbonized EWC was impregnated with concentrated phosphoric acid (H_3PO_4) at a weight ratio of 1:3 (carbon:acid) and soaked for 24 h to ensure thorough activation. After impregnation, the sample was repeatedly washed with deionized water until the filtrate reached a neutral pH. The washed material was then oven-dried at 120 °C for 12 h and subsequently thermally activated at 800 °C for 1 h in a muffle furnace. The obtained EWAC was cooled to room temperature, sealed in airtight containers, and used for subsequent characterization and adsorption experiments.

3) Materials and reagents

The physicochemical properties of the prepared adsorbents were characterized via various analytical techniques. The crystalline structure and phase composition of the ACwere analyzed via X-ray diffraction (XRD) via a Bruker AXS D8 diffractometer equipped with Cu-Kα radiation (λ = 1.5406 Å). Textural characteristics, including specific surface area and pore volume, were determined via nitrogen adsorption–desorption analysis at 77 K via a VSorb 2800P surface area analyzer (Gold APP Instruments, China). The Brunauer–Emmett–Teller (BET) method was applied to calculate the surface area, whereas the Barrett–Joyner–Halenda (BJH) model was used to determine the pore size distribution. The surface functional groups of the samples were identified via Fourier transform infrared (FTIR) spectroscopy via a PerkinElmer Spectrum One spectrometer (USA) within the wavenumber range of 4,000–400 cm^{-1}. The elemental composition (C, H, O, and N) was analyzed via a CHON elemental analyzer (LECO 628 Series, China). Additionally, the pH at the point of zero charge (pHpzc) of the adsorbent was determined via the acid–base titration method as described in previous study (Rockwood et al. 2019).

4) Materials and reagents

RockwoodBatch adsorption experiments were performed in 125 mL Erlenmeyer flasks using a mechanical shaker operated at 250 rpm to evaluate the influence of various operational parameters. The investigated parameters included initial pH (3–8), adsorbent dosage (0.01–0.50 g per 50 mL of MO solution), contact time (5–720 min), initial dye concentration (5–600 mg L^{-1}), and temperature (20–40 °C). The particle size of the adsorbent ranged from 2–4 μm. The pH of each solution was adjusted with 0.1 M HCl or NaOH as needed.

During the adsorption process, aliquots of the suspension were collected at predetermined time intervals and filtered through a 0.45 μm micromembrane to separate the adsorbent from the aqueous phase. The residual dye concentration in the filtrate was determined via a UV–visible spectrophotometer (UV-1800, Shimadzu, Japan) at the maximum absorption wavelength (λmax) of 497 nm. All experiments were conducted in triplicate, and the mean values are reported.

The dye removal efficiency (% R) and adsorption capacity at equilibrium (q_e, mg g^{-1}) were calculated via the following equations (Eqs.1-2).

$$(\%R) = [(C_0 - C_e)/C_0] \times 100 \quad \text{(Eq.1)}$$

$$q_e = V(C_0 - C_e)/m \quad \text{(Eq.2)}$$

where C_0 (mg L^{-1}) and C_e (mg L^{-1}) are the initial and equilibrium dye concentrations, respectively; V (L) is the volume of the dye solution; and m (g) is the mass of the adsorbent used (Suma et al., 2021).

5) Adsorption kinetics

Adsorption kinetics play a crucial role in adsorption process design, as they determine the rate and efficiency of solute uptake and provide insight into the mechanism and rate-controlling steps. To investigate the adsorption kinetics of MO on the prepared adsorbent, batch experiments were performed under controlled conditions. The initial dye concentrations were varied at 20, 60, and 100 mg L^{-1}, and the pH was maintained at 4. The adsorbent dosage was fixed at 0.2 g per 50 mL of MO solution, and the temperature was maintained at 30 °C. The contact time ranged from 5 to 720 min to ensure equilibrium was reached.

The experimental kinetic data were analyzed via pseudo-first-order and pseudo-second-order models, expressed by Eq. (3) and Eq. (4), respectively (Suma et al., 2021).

Pseudo-first-order model:

$$\ln(q_e - q_t) = \ln q_e - k_1 t \quad \text{(Eq.3)}$$

Pseudo-second-order model:

$$t/q_t = (1/k_2 q_e) + (1/q_e)t \quad \text{(Eq.4)}$$

where q_e and q_t are the adsorption capacities of MO at equilibrium and at time (mg g^{-1}), respectively. The symbol t represents the adsorption time (min). The pseudo-first-order (1 min^{-1}) and pseudo-second-order (g mg^{-1} min^{-1}) rate constants are k_1 and k_2, respectively.

The pseudo-first-order model is applied to describe the initial stage of the adsorption process, assuming that one dye molecule is adsorbed onto a single active site on the adsorbent surface. In contrast, the pseudo-second-order model is based on the assumption that the rate-limiting step involves chemisorption, in which valence forces arise from the sharing or exchange of electrons between the adsorbate and the adsorbent (Phothitontimongkol and Prasertboonyai, 2024).

Moreover, the Weber–Morris intraparticle diffusion model was used, and the definition of this model is shown in Eq.5 (Moghaddasi et al., 2010) to obtain more details related to the adsorption mechanism and to explain the rate-controlling step of MO adsorption onto EWACs.

$$Q_t = k_i t^{1/2} + C \quad \text{(Eq.5)}$$

where ki represents the constant for intraparticle diffusion and where C denotes the intercept indicating the thickness of the boundary layer. The Weber–Morris intraparticle diffusion model is employed to determine

whether intraparticle diffusion governs the adsorption rate. A linear relationship between q_t and $t^{1/2}$ indicates diffusion-controlled adsorption; however, deviation from linearity or a nonzero intercept suggests that additional mechanisms, such as external film diffusion, also contribute. The intercept C reflects the boundary layer thickness and the extent of surface adsorption (Phothitontimongkol and Prasertboonyai, 2024).

6) Adsorption isotherm

Adsorption isotherms provide essential information on the distribution of adsorbate molecules between the liquid and solid phases at equilibrium, offering insight into surface properties and adsorption mechanisms. Analyzing equilibrium data via various isotherm models is critical for identifying the most suitable model for describing adsorption behavior and guiding process design.

In this study, two widely applied isotherm models—the Langmuir and Freundlich models—were used to evaluate the equilibrium adsorption of MO onto EWAC. The Langmuir isotherm model assumes a homogeneous adsorbent surface with energetically identical adsorption sites and monolayer coverage, implying that the adsorbed molecules do not interact with one another (Luo et al., 2019). In contrast, the Freundlich isotherm model is an empirical relationship that represents solute adsorption from a liquid phase onto a solid surface. This model assumes a heterogeneous adsorbent surface with adsorption sites of different energies, allowing for multilayer adsorption (Luo et al., 2019). The isotherm experiments were conducted at an initial pH of 4, using an adsorbent dose of 0.2 g per 50 mL of MO solution, a contact time of 30 min, initial dye concentrations ranging from 5 to 600 mg L^{-1}, and temperatures between 20 and 40 °C. The obtained equilibrium data were fitted to the Langmuir and Freundlich equations to elucidate the adsorption mechanism and surface interaction characteristics of the EWAC. The equations of the adsorption models are provided in Eq.6 and Eq.7.

Langmuir isotherm model:

$$C_e/q_e = (1/K_L q_m) + 1/q_m C_e \quad \text{(Eq.6)}$$

Freundlich isotherm model:

$$\ln q_e = 1/n \ln C_e + \ln K_F \quad \text{(Eq.7)}$$

In the provided equations, q_m (mg g^{-1}) represents the theoretical maximum adsorption capacity, K_L (L mg^{-1}) signifies the Langmuir isotherm constant, C_e denotes the equilibrium concentration (mg L^{-1}), and K_F (mg g^{-1}) and n represent the Freundlich isotherm constant and heterogeneity factor, respectively. These parameters characterize the adsorbent's adsorption intensity.

7) Thermodynamic studies

This investigation investigated the effect of temperature on the adsorption of MO onto the EWAC adsorbent, encompassing equilibrium trials conducted, ranging from 293.15 K to 313.15 K, while the initial concentrations of the dye solutions were varied. The parameters of the adsorption isotherm model were subsequently acquired at various temperatures, facilitating the computation of various thermodynamic parameters, such as the changes in Gibbs free energy (ΔG), enthalpy (ΔH), and entropy (ΔS), associated with the process. Using Eq. 8, the Langmuir isotherm parameter, K_L, was used to determine the adsorption equilibrium constant, K_a (L g^{-1}).

$$K_a = q_{max} K_L \quad \text{(Eq.8)}$$

The ΔS, ΔH, and ΔG values were calculated according to Eq.9 and Eq.10.

$$\Delta G = -RT\ln(K_a) \quad \text{(Eq.9)}$$

$$\ln K_a = (\Delta S/R) - (\Delta H/RT) \quad \text{(Eq.10)}$$

where T represents the absolute temperature in (K) and represents the universal gas constant (J $mole^{-1}$ K^{-1}).

8) Regeneration and reusability studies

The regeneration and reusability performance of the optimized adsorbent were evaluated over seven consecutive adsorption–desorption cycles. During each adsorption cycle, MO solution with an initial concentration of 20 mg L^{-1} was used at 25.0 ± 1.0 °C. The adsorbent dosage and solution volume were increased threefold to 2 g and 250 mL, respectively. The adsorption experiments were conducted at a constant pH of 4.0 with agitation at 250 rpm for 60 min. After each adsorption step, the adsorbent was separated by centrifugation and regenerated by immersion in 100 mL of 0.1 M NaOH solution for 1 h to facilitate the desorption of the adsorbed dye molecules. The regenerated adsorbent was repeatedly washed with deionized water until the wash solution reached neutral pH and then dried in a hot-air oven at 110 °C for 12 h. This adsorption–desorption cycle was repeated seven times, and the dye removal efficiency (% R) was calculated via Eq.1.

Results and discussion

1) Characterization of the EWAC

Figure 1a shows the XRD patterns of GAC, EWC, and EWAC. The raw GAC exhibited two major broad peaks at 2θ at approximately 25.56° and 44.54° corresponding to the amorphous carbon and layer aromatic carbon phases, respectively. There were some small peaks at 2 θ values of approximately 18.1°, 26.1°, 29.1° and 33.8° attributed to calcium carbonate ($CaCO_3$) embedded inside the

wood. After being treated in H3PO4 solution, the EWC sample contained predominantly amorphous carbon and layered aromatic carbon phases with minor impurities of $CaCO_3$. After activation, only two broad peaks at 2 θ values of approximately 25.56° and 44.54° were dominant, suggesting the major formation of amorphous carbon and layered aromatic carbon phases. This result could imply that the synthesis of EWAC was successful.

Figure 1b shows the FT-IR spectra, revealing the presence of abundant functional groups in the adsorbents. The spectrum of EWC exhibited distinct functional groups of oxygen-containing and aromatic compounds, such as C=C stretching at approximately 1,540 cm^{-1}, C=O stretching at approximately 1,620 cm^{-1}, C–H stretching of the methylene group ($–CH_2$) at 2915 cm-1 and O–H stretching at 3,420 cm^{-1}. Following H3PO4 treatment of the EWC and subsequent thermal activation at 800 °C, the EWAC displayed fewer peaks (3,420 and 2,915 cm^{-1}) than did the EWC, which was attributed primarily to the loss of volatile compounds during pretreatment. Compared with the FT-IR spectra of H3PO4-treated EWC and thermally activated EWAC, the alcoholic/phenolic O–H stretching peak was less intense and shifted to greater energy (3,420 cm^{-1}), suggesting the disruption of hydrogen bonds and the loss of bound moisture through pyrolysis. The carbonyl peak decreased in intensity but shifted to lower energy (approximately 1,620 cm^{-1}), suggesting pyrolysis-induced loss of the carbonyl functional group, with a majority being directed toward pyrolysis oil rather than biochar (Chu et al., 2018). There are notable peaks at approximately 1200 cm-1, which could indicate the stretching mode related to hydrogen-bonded P=O, the O-C stretching vibration within P-O-C (aromatic) linkages, and the existence of P=OOH bonds (Jagtoyen et al., 1998). Additionally, the band at 1,087 cm^{-1} could be attributed to vibrations stemming from ionized P±-O- in acid phosphate esters and the symmetrical P-O-P vibration found in polyphosphate compounds (Sych et al., 2012). Moreover, the adsorption of MO appears to influence the rearrangement of functional groups, as evidenced by shifts observed in the FT-IR spectra of EWAC before and after MO adsorption. On the basis of this analysis, it can be inferred that the C=O, C=C, and C-C groups play a role in the binding of MO to EWAC (Zein et al., 2023).

The porosity characteristics of EWC and EWAC impregnated with different amounts of H_3PO_4 via the N2 sorption technique are shown in Table 1. The N_2 adsorption/desorption isotherms and pore size distributions of the EWAC (1:3) samples are shown in Figure 1c and 1d. When the impregnation ratios of EWC and H3PO4 increased from 1:1 to 1:3, the sample BET surface area and percentage of MO removal increased and became nearly constant when the impregnation ratio reached 1:3. In summary, these data may indicate that the use of H_3PO_4 as a chemical agent to promote the decomposition of carbonaceous char during activation is likely the reason why the increase in acid concentration results in an increase in the BET surface area. Furthermore, MO removal from all the adsorbents was investigated, and the results are shown in Table 1. The surface area of the adsorbent increased, and the percentage of removal increased noticeably. Notably, the slightly improved MO removal for the 1:4 sample, despite a lower surface area, might be attributed to enhanced surface acidity, phosphorus-containing functional groups, and improved pore accessibility, which can outweigh surface area effects (Phothitontimongkol, and Prasertboonyai, 2024)

However, in terms of economic value, EWAC-3:1 was selected as the best adsorbent for further study because of its high MO removal efficiency and lower consumption of H_3PO_4.

The surface area of AC was assessed via the BET equation. The external surface area and micropore area were determined via the T-plot method. Moreover, the total pore volume was determined by measuring the quantity of N_2 adsorbed at a specific relative pressure, whereas the mesopore volume was calculated by subtracting the micropore volume from the total pore volume. In Table 1, the physicochemical properties of the EWAC are delineated. The EWAC displays both micropore (<2 nm) and mesopore (2–50 nm) structures; notably, the micropore volume (V_{micro}) constitutes approximately 70% of the total pore volume, surpassing the mesopore volume. Smaller particle sizes are associated with improved rates of diffusion and adsorption in porous carbon.

The elemental content of the EWAC was thoroughly examined and contrasted with that of the EWC, as illustrated in Table 2. Notably, the proportions of C/H and C/O in the EWAC are substantially greater than those in the EWC, indicating the increased hydrophobicity of the material. This increased hydrophobicity of the adsorbent could facilitate the adsorption of MO, particularly in nonpolar regions such as the aromatic ring.

2) Effect of pH

The point of zero charge (pHPZC) is a key parameter governing the surface charge of adsorbents and thus their adsorption behavior (Figure 2a). The pHPZC of the EWAC was found to be between pH 4.0 and 5.5. As shown in Figure 2b, MO removal increased with increasing pH and reached a maximum at pH 4, after which further pH elevation led to a decrease in removal efficiency. This pH-dependent behavior arises from changes in the surface charge of the EWAC relative to its pHPZC, which controls electrostatic attraction or repulsion between the charged surface sites and MO molecules (Phothitontimongkol and Prasertboonyai, 2024)

Table 1 Porosity characteristics of EWC and EWAC impregnated with different amounts of H_3PO_4 as assessed through the N_2 sorption technique

Adsorbents	S_{BET}[1] (m^2 g^{-1})	V_t[2] (cm^3 g^{-1})	V_{micro}[3] (cm^3 g^{-1})	Pore size[4] (nm)	Removal (%)
EWC	89.77	0.07	0.02	3.01	9.78
EWAC-1:1	291.87	0.18	0.12	2.25	30.54
EWAC-1:2	547.36	0.29	0.20	2.13	67.94
EWAC-1:3	1027.78	0.49	0.35	1.99	81.45
EWAC-1:4	875.89	0.42	0.33	1.90	83.23

Remark: [1] Measured via the BET method.
[2] Total pore volume determined at P/P_0 = 0.9955.
[3] Volume of micropores calculated via the *t* plot method,and $V_{meso} = V_t - V_{micro}$.
[4] Pore size analysis via the BJH method.

Table 2 Elemental composition assessed via CHNO analysis of EWC and EWACs.

Adsorbents	Elemental (%)				Element ratio	
	C	H	N	O	C/H	C/O
EWC	52.18	8.03	0.09	39.70	6.50	1.31
EWAC-1:3	71.93	2.71	0.85	24.51	26.54	2.93

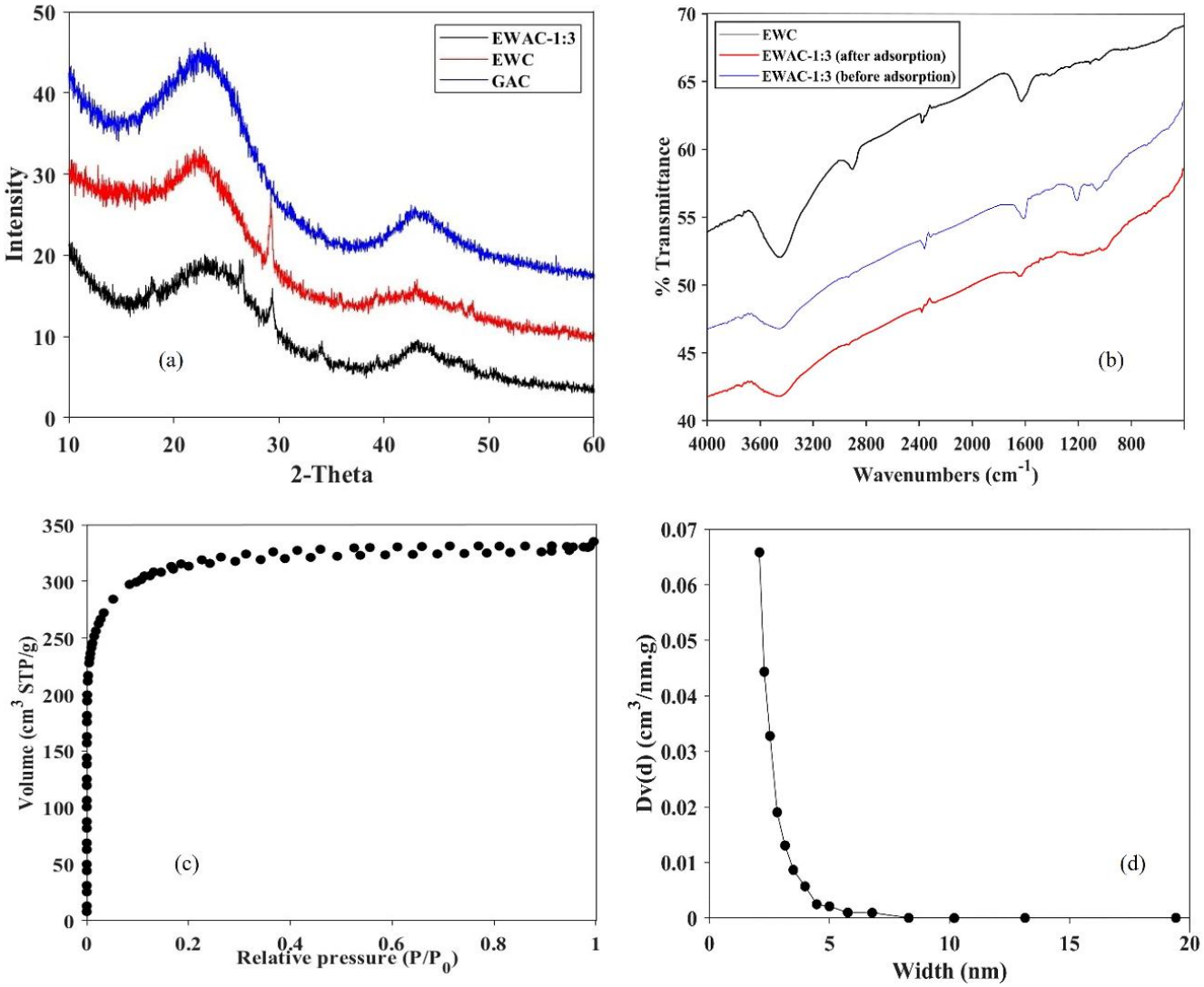

Figure 1 XRD patterns (a) and FTIR spectra (b) of GAC, EW and EWAC, (c) N_2 adsorption/desorption isotherms and (d) pore size distributions of the EWAC.

The strong dependence of MO adsorption on pH confirms that electrostatic interactions play a dominant role in the adsorption mechanism. At pH values below the pHPZC of EWAC, protonation of surface functional groups generates positively charged adsorption sites, which increase the electrostatic attraction toward anionic MO molecules. At higher pH values, deprotonation of the surface leads to electrostatic repulsion, thereby reducing the adsorption efficiency (Moghaddasi et al., 2010; Phothitontimongkol, and Prasertboonyai, 2024). These observations indicate that surface charge regulation, rather than surface area alone, governs MO uptake under various pH conditions. Hence, a pH of 4.0 was selected for further experiments.

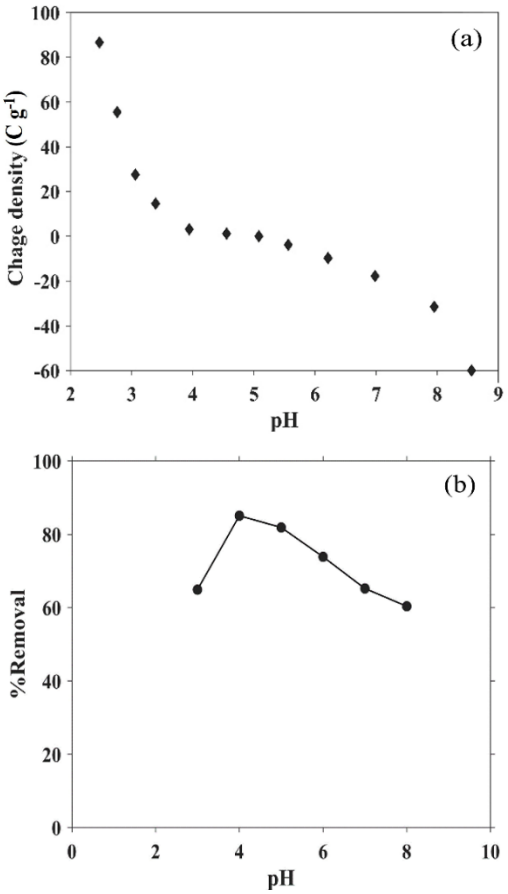

Figure 2 (a) pH_{PZC} effect on EWAC, (b) effect of pH on MO adsorption (C_0 = 20 mg L^{-1}, adsorbent dose = 0.2 g in 50 mL of MO solution and contact time = 30 min at 25 °C.

3) Effect of adsorbent dose

Figure 3 shows the correlation between MO removal and adsorbent dose. The sample doses were in the range of 0.01–0.5 g per 50 mL of MO solution. The results demonstrate a significant increase in the percentage of MO dye removed, reaching 100%, with higher adsorbent doses. This increase can be attributed to the increased adsorbent dose, leading to an increased adsorption area. However, the adsorption capacity per unit mass (q_e) of the adsorbent decreased as the adsorbent dose increased. Considering financial constraints, we determined the optimal adsorbent dose for EWACs to be 0.2 g per 50 mL of MO solution, resulting in an adsorption capacity of 4.66 mg g^{-1} and an approximately 94% removal percentage.

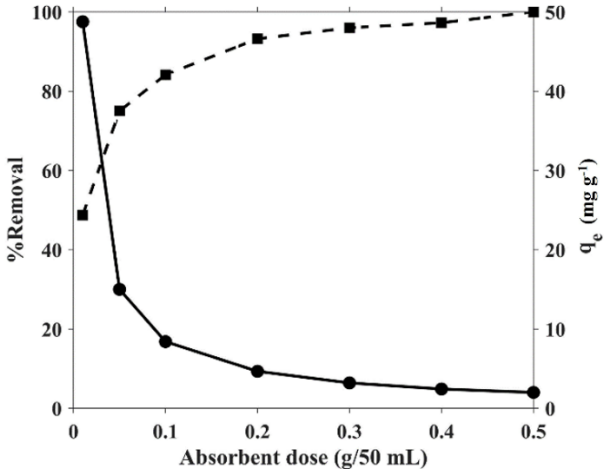

Figure 3 Effect of adsorbent dose (C_0 = 20 mg L^{-1}, pH = 4, contact time = 30 min at 25 °C)

4) Effects of contact time and adsorption kinetics

The duration of contact plays a pivotal role in optimizing treatment processes. The samples were tested for their ability to adsorb the dye during contact while the pH was maintained at 4 and the dye concentration was 20 mg L^{-1}. Figure 4a illustrates how the removal of dye by EWAC varied over contact times ranging from 5–720 min. Initially, there was a swift increase in MO removal, followed by a plateau until approximately 30 min, indicating stabilization of the adsorption rate, which was considered the equilibrium point. This initial rise can be attributed to the availability of numerous active sites on the adsorbent surface before dye molecules occupy them during adsorption. This finding also suggests rapid adsorption of adsorbate species initially, followed by a slower approach toward equilibrium.

Figure 4b to 4d depict the linear pseudo-first-order kinetics, pseudo-second-order kinetics, and intraparticle diffusion plots. The results of the analysis in Table 3 suggest that the pseudo-second-order model offers a superior fit to the experimental data compared with the pseudo-first-order model. Therefore, the pseudo-second-order model accurately predicts the adsorption of MO by EWACs. The primary mechanism identified for MO adsorption by EWACs is chemical adsorption, involving valence forces or electron exchange between MO and surface groups in EWACs.

The correlation between q_t and $t_{1/2}$ according to the intraparticle diffusion model reveals several linear phases involved in the MO removal process by EWAC. Initially, a stage denoted film/surface diffusion occurred, where MO molecules diffused across the liquid film and promptly adhered to the external surface of the EWAC.

The relatively high values of the intraparticle diffusion rate constant (k_i) alongside the relatively low values of the EWC suggest that the EWAC has an abundant surface area and active sites. In the subsequent phase of intraparticle diffusion, MO molecules penetrate into the pores on the internal surface of AC (Moghaddasi et al., 2010). The final phase represents the adsorption equilibrium of MO molecules on EWAC, characterized by the lowest k values, indicating a slowdown in intraparticle diffusion due to the low residual MO concentration in the solution and the limited availability of free active sites (Moghaddasi et al., 2010).

Table 3 Kinetic parameters for MO adsorption by EWACs (C_0 = 20 mg L^{-1}, pH = 4, adsorbent dose = 0.2 g in 50 mL of MO solution at 25 °C)

$q_{e,exp}q_{e,exp}$ (mg g^{-1})	Pseudo-first-order			Pseudo-second-order			Interparticle diffusion		
	K_1 (1 min^{-1})	$q_{e,cal}$ (mg g^{-1})	R^2	K_2 (g mg^{-1} min^{-1})	$q_{e,cal}$ (mg g^{-1})	R^2	K_i (mg g^{-1} $min^{-1/2}$)	C	R^2
5.02	0.0084	4.556	0.9832	0.269	5.038	0.9999	0.8443	0.1985	0.9941

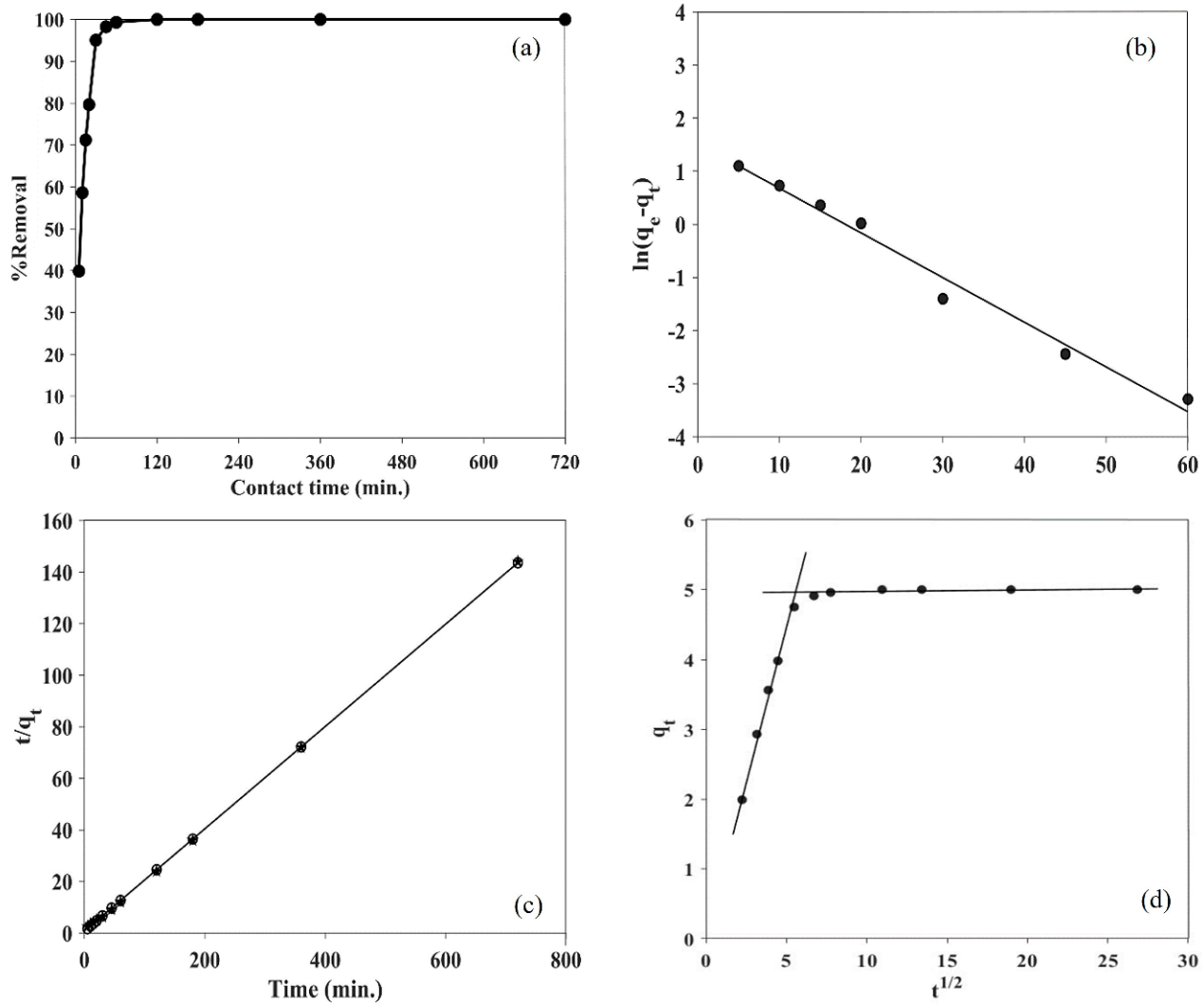

Figure 4 Effect of contact time (a), pseudo-first-order kinetics (b), pseudo-second-order kinetics (c), and intraparticle diffusion (d) for MO removal via the EWAC adsorbent. (C_0 = 5–600 mg L^{-1}, pH = 4, adsorbent dose = 0.2 g in 50 mL of MO solution, and temperature = 25 °C)

5) Effect of initial dye concentration and adsorption isotherms

The influence of the initial dye concentration within the range of 5–600 mg L^{-1} was investigated. As illustrated in Figure 5, the percentage of MO removed by AC decreased as the initial concentration increased because of the saturation of the active sites from 5 to 300 mg L^{-1}, beyond which the percentage removal slightly decreased. This decline in percentage removal can be attributed to adsorbents having a finite number of adsorption sites and then being saturated at a specific concentration. In contrast, the adsorption capacity of EWAC increased at various initial MO concentrations. The enhanced dye uptake capacity is typically linked to the notion that a

heightened concentration gradient furnishes a stronger impetus to surmount all mass transfer hindrances of the dye molecules between the aqueous and solid phases. This leads to an elevated equilibrium uptake capacity before adsorbent saturation is reached. Adsorption isotherm models were utilized to characterize the adsorption behavior of MO onto EWAC.

The Langmuir isotherm describes monolayer adsorption over a uniform adsorbent surface, assuming consistent energies of adsorption across the surface. On the other hand, the Freundlich model applies to adsorption systems on heterogeneous surfaces where the energy of adsorption varies across the adsorbent surface sites. The adsorption equilibrium data fitted with the Langmuir and Freundlich models are depicted in Figure 5, and the isotherm parameters, including coefficients (R^2), are summarized in Table 4. When the regression coefficients (R^2) obtained from both models were compared, the R^2 value of the experimental data fit well with the Langmuir model rather than the Freundlich model. A higher R^2 value could indicate better applicability and reliability of a given model. This result suggests monolayer coverage of MO on the homogeneous surface of the adsorbents. Moreover, the maximum adsorption capacity of the EWAC sample for MO was approximately 29.11 mg g^{-1} at 25 °C.

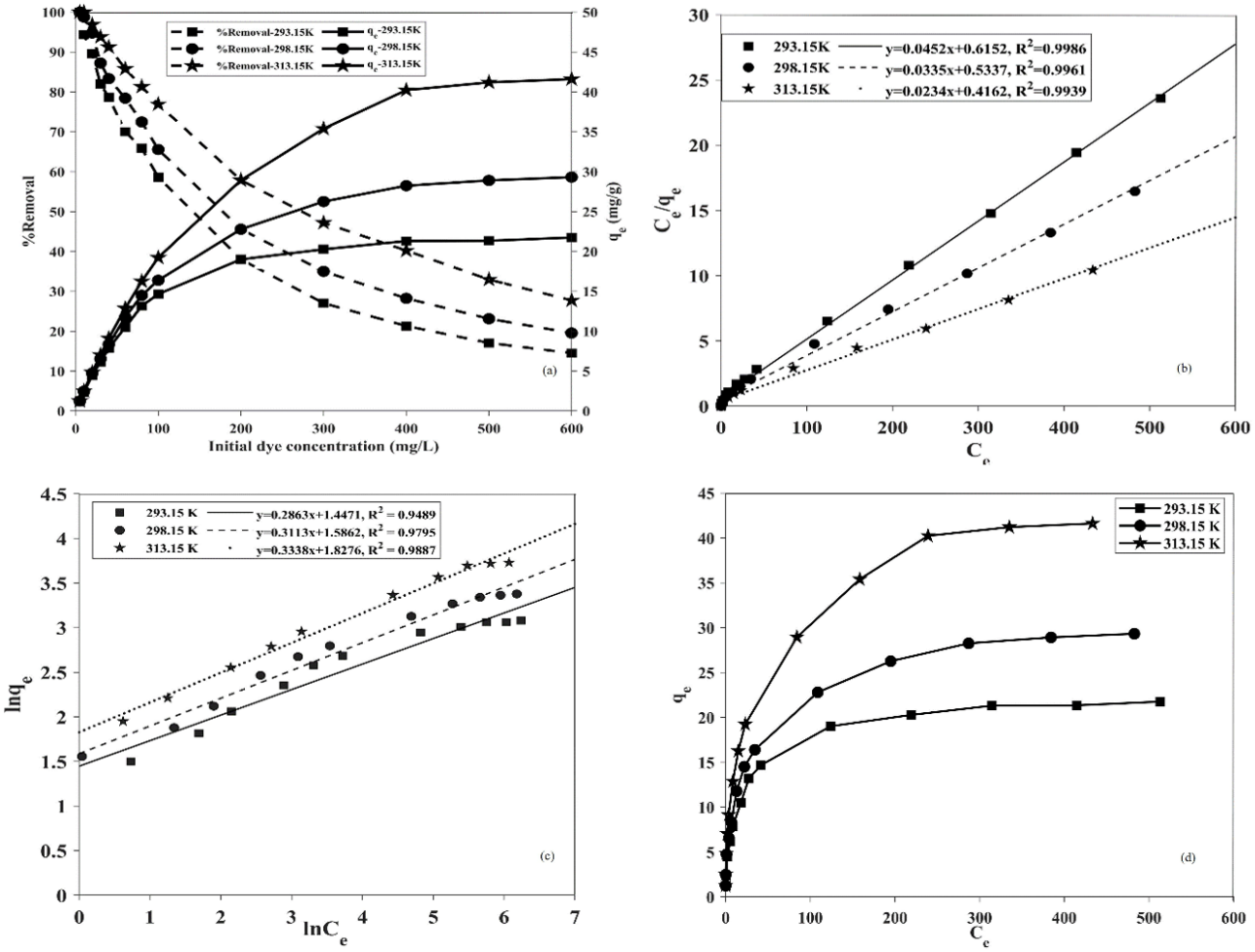

Figure 5 Effect of initial MO concentration (a), Langmuir isotherms (b), Freundlich isotherms (c), and plot of C_e versus q_e (d) for MO adsorption onto EWAC at different initial dye concentrations (pH = 4, adsorbent dose = 0.2 g per 50 mL of MO solution, contact time = 30 min)

Table 4 Constant parameters and correlation coefficients calculated for different adsorption models at various initial MO concentrations

T (K)	$q_{e,exp}$ (mg g^{-1})	Langmuir			Freundlich			Thermodynamic		
		q_m (mg g^{-1})	K_L (mg g^{-1})	R^2	K_F (mg g^{-1})	1/*n*	R^2	ΔG (kJ mol^{-1})	ΔH (kJ mol^{-1})	ΔS (kJ mol^{-1} K^{-1})
293.15	21.47	22.12	0.073	0.9986	4.25	0.286	0.9489	-1.167		
298.15	29.11	29.85	0.063	0.9961	4.89	0.311	0.9795	-1.565	14.746	0.0545
313.15	41.02	43.10	0.056	0.9939	6.22	0.334	0.9887	-2.293		

6) Effects of temperature and thermodynamics

To explore the influence of temperature on MO adsorption onto AC, experiments were conducted at temperatures ranging from 20 °C to 45 °C, and the findings are shown in Figure 6. The results revealed that when the adsorption temperature increased, the adsorption capacity of MO improved. This observation could be the consequence of the enhanced mobility of MO molecules, which promotes greater interactions between MO and EWAC, implying an endothermic nature of adsorption (Moghaddasi et al., 2010).

In Figure 5b, the plot of q_e against Ce at different temperatures reveals a positive correlation between qe and temperature. The calculated maximum adsorption capacity (q_{max}) of MO by the adsorbent increased from 22.12 to 43.10 mg g^{-1} ($q_{e,exp}$ = 21.47 to 41.02 mg g^{-1}) as the temperature increased from 293.15 K to 313.15 K, indicating the endothermic nature of the adsorption process. This trend could be the consequence of the enhanced diffusion of MO throughout the external boundary layer and within the internal pores of the solid adsorbent particles at higher temperatures. Consequently, a greater amount of MO molecules could gain adequate energy to engage with binding sites on the surface of the particles. A van't Hoff plot was generated to study the thermodynamic parameters, and the results are presented in

Table 4 The reduction in the ΔG and more negative values when the temperature increased suggested that the adsorption process became feasible and spontaneous. The positive ΔS value (0.0545 kJ mol^{-1} K^{-1}) implies that the increased randomness of dye molecules on the surface of the adsorbent particles compared with the dye solution facilitates interactions between the solid and liquid phases. Furthermore, the positive ΔH value (14.746 kJ mol^{-1}) supports the endothermic nature of the adsorption process under investigation, which aligns with earlier observations of increased q_e values with increasing temperature (Palapa et al., 2021).

7) Comparative interpretation of pH, kinetic, and temperature effects

Overall, the adsorption behavior of MO onto EWAC is governed by a combination of electrostatic interactions, diffusion processes, and temperature-dependent adsorption energetics. The strong pH dependence indicates that surface charge regulation plays a dominant role, with enhanced adsorption occurring at pH values below the pHPZC due to electrostatic attraction between negatively charged MO molecules and protonated functional groups on EWACs. Kinetic analysis further suggested that chemisorption involving electron sharing or exchange between MO and surface functional groups is the rate-limiting step, whereas intraparticle diffusion analysis revealed that a multistage adsorption process is controlled initially by external film diffusion followed by gradual pore diffusion. In addition, the observed increase in adsorption capacity with temperature confirms the endothermic nature of the process, as elevated temperatures enhance molecular mobility, reduce mass-transfer resistance, and promote stronger adsorbate–adsorbent interactions. Additionally, these results demonstrate that MO adsorption on EWAC is controlled by synergistic surface chemistry and transport phenomena rather than surface area alone.

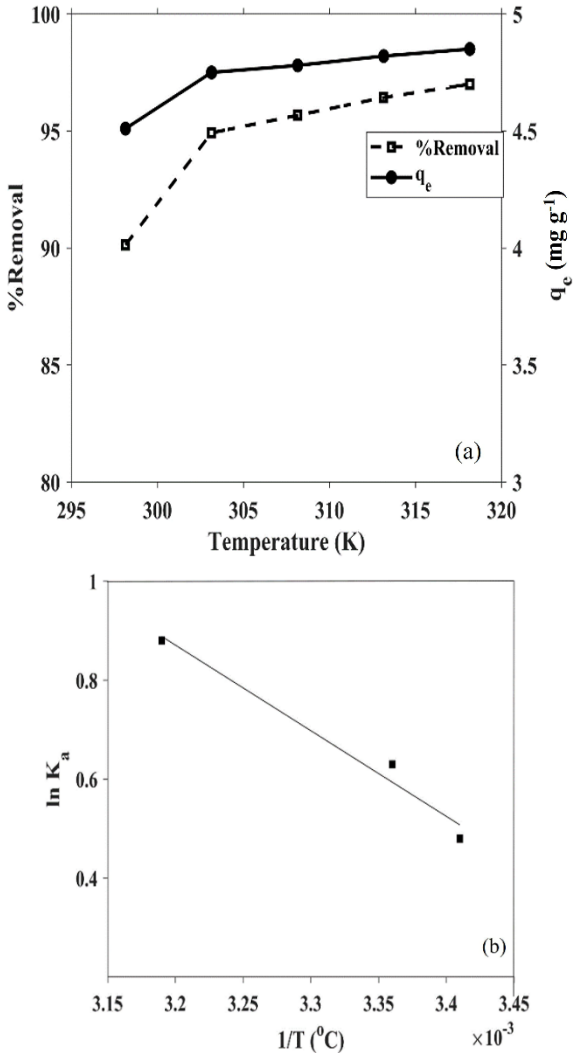

Figure 6 Effects of temperature (a) and the van't Hoff plot (b) for MO removal via the EWAC adsorbent (pH = 4, adsorbent dose = 0.2 g per 50 mL of MO solution, contact time = 30 min at 25 °C)

8) Regeneration and reusability studies of adsorbents

The reusability and regeneration efficiency of the best adsorbent are shown in Figure 7, and seven adsorption–desorption cycles were performed. In this work, alkaline desorption using NaOH disrupts electrostatic and hydrogen bonding interactions between MO molecules and EWACs (Phothitontimongkol and Prasertboonyai, 2024). The regeneration of adsorbed molecules from EWAC is highly important because it directly impacts the cost-effectiveness of the adsorption process. As shown in Figure 7, the percentage of MO removed by the EWAC

remains relatively stable up to the 4th cycle. The gradual decline observed in the 6th and 7th cycles is attributed to partial blockage of pores, loss of surface functional groups, and structural fatigue caused by repeated adsorption–desorption cycles. This phenomenon seems consistent with our previous findings that the reusability of MO removal on AC produced from Tammarine wood could also preserve the original removal efficiency up to the 4th cycle and drastically decrease in the 5th cycle (Phothitontimongkol and Prasertboonyai, 2024).

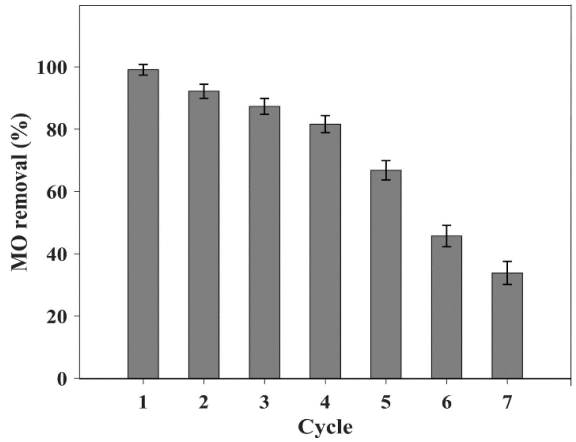

Figure 7 Cycles of regeneration and reusability of EWAC.

9) Comparison of MO adsorption using various adsorbents

Table 5 shows a comparison of the maximum MO adsorption capacities of the different adsorbents compared with those reported in the relevant literature. Among various adsorbents with similar adsorption conditions, the EWAC provided the maximum adsorption capacity of MO, which was in the same range as that reported in the relevant literature but had a reusability capacity of up to the 6th cycle. This result suggests that the EWAC is accessible and cost effective for water treatment and could be further beneficial, making it a preferred choice for removing MO from aqueous solutions.

Consequently, the observed q_{max} in Table 4 (~29 mg g^{-1} at 298 K) is consistent with many biomass-derived activated carbons reported in Table 5 (Djilani et al., 2015; Mohamed et al., 2021; Pal et al., 2013; Phothitontimongkol and Prasertboonyai, 2024), whereas higher temperatures enhance diffusion/accessibility and increase q_{max} to ~43 mg g^{-1} at 313 K, confirming that adsorption is strongly condition- and structure-dependent rather than solely controlled by the BET surface area.

Although EWAC has a high BET surface area (~1,027 m^2 g^{-1}), the adsorption capacity is governed not only by the surface area but also by the pore size distribution, surface chemistry, and adsorbate–adsorbent interactions [38,39]. In this study, the EWAC contains a high fraction of micropores (<2 nm), which may limit accessibility for relatively large MO molecules. Additionally, adsorption is dominated by specific interactions (electrostatic and chemical adsorption) rather than purely physical adsorption, thereby limiting the maximum uptake.

Compared with commercial activated carbon (CAC) (Dehmani et al., 2025; Djilani et al., 2015; Kumar et al., 2023; Mohamed et al., 2026; Pal et al., 2013), which is widely reported to have higher MO adsorption capacities due to a more balanced meso–micropore structure and greater surface area. Therefore, the EWAC is not designed to compete directly with premium commercial or engineered adsorbents in terms of maximum adsorption capacity alone. Instead, its advantages include low-cost feedstock, waste valorization, simple preparation, and environmental sustainability, which are critical factors for large-scale wastewater treatment applications. These results highlight the trade-off between adsorption performance and material cost/complexity and underscore the potential of EWAC as a sustainable alternative adsorbent rather than a high-end specialty material.

Table 5 Comparison of MO adsorption conditions and the maximum capacity observed in this study with those reported in the relevant literature

Adsorbent from various natural wastes (AC source)	Adsorbate concentration range (mg L^{-1})	Reuse ability	Maximum adsorption capacity (mg g^{-1})	References
Waste tamarind wood	10-500	6	39.4	Phothitontimongkol and Prasertboonyai (2024)
Camel Thorn Plant	5-80	-	24.0	Mohamed et al. (2021)
Apricotstones	20-300	-	32.2	Djilani et al. (2015)
AgNPs-coated activated carbon	20-100	10	27.5	Pal et al. (2013)
Residual eucalyptus wood	5-600	6	29.1	This study
CAC	20-500	-	100	Dehmani et al. (2026)
CAC	20-300	-	81	Djilani et al. (2015)

Conclusions

Eucalyptus wood–based activated carbon (EWAC) was successfully synthesized via pyrolysis and demonstrated excellent performance as an adsorbent for the removal of MO dye from aqueous solution. FTIR analysis confirmed the presence of abundant oxygen- and phosphorus-containing functional groups (–OH, C=O, P=O, and P–O–C), which provided active sites for dye adsorption through electrostatic attraction, hydrogen bonding, and π–π interactions. The XRD results revealed that the amorphous carbon structure of the EWAC favored dye uptake by offering high surface reactivity. The adsorption performance of the EWAC improved with increasing pH, adsorbent dosage, contact time, and temperature. Kinetic studies revealed that the adsorption process followed a pseudo-second-order model, suggesting that chemisorption governed the rate-limiting step. The equilibrium data were best fitted by the Langmuir isotherm model, indicating monolayer adsorption with a maximum capacity of 29.11 mg g^{-1} at 303.15 K. The thermodynamic parameters demonstrated that the adsorption was endothermic, spontaneous, and more favorable at elevated temperatures. Furthermore, regeneration experiments confirmed that EWAC maintained considerable adsorption efficiency after at least four consecutive cycles, emphasizing its potential as a cost-effective, eco-friendly, and sustainable adsorbent for the treatment of dye-contaminated wastewater.

Acknowledgements

The authors would like to express their sincere appreciation to the Faculty of Science, Energy and Environment, King Mongkut's University of Technology North Bangkok, for providing the laboratory facilities and support necessary to conduct this research. This work was financially supported by the National Science, Research and Innovation Fund (NSRF) and King Mongkut's University of Technology North Bangkok under Contract No. KMUTNB-FF-66-59.

Data availability statement

Information and data used in the study will be disclosed upon request.

Author ORCID

Mathin Jaikua: 0009-0007-3956-3758
Phuthidhorn Thana: 0000-0002-9736-7364
Sunisa Ungwiwatkul: 0000-0002-4762-8079
Jakkrawut Maitip: 0000-0001-6265-1421
Kanyarak Prasertboonyai: 0000-0002-7089-034X

Author contributions

Mathin Jaikua: Investigation, Resources, Project administration
Phuthidhorn Thana: Investigation, Resources
Sunisa Ungwiwatkul: Investigation, Resources
Jakkrawut Maitip: Resources, Project administration, Funding acquisition
Kanyarak Prasertboonyai: Conceptualization, Methodology, Validation, Formal analysis, Investigation, Resources, Data curation, Writing – Original draft, Writing – Review & editing, Visualization, Supervision

Conflicts of interest

The authors declare that they are no known competing financial interests or personal relationships that could have appeared to influence the work reported in this paper.

References

Bella, H., & Bendaikha, H. (2022). Biochar from empty date fruit bunch as an adsorbent to remove eriochrome black T and methylene blue from aqueous solution. *Applied Environmental Research*, *44*(2), 44–55.

Brito, M. J. P., Veloso, C. M., Santos, L. S., Bonomo, R. C. F., & F ontan, R. D. C. I. (2018). Adsorption of the textile dye Dianix® royal blue CC onto carbons obtained from yellow mombin fruit stones and activated with KOH and H_3PO_4: Kinetics, adsorption equilibrium and thermodynamic studies. *Powder Technology*, *339*, 334–343.

Chen, Y., Zhai, S. R., Liu, N., Song, Y., An, Q. D., & Song, X. W. (2013). Dye removal of activated carbons prepared from NaOH-pretreated rice husks by low-temperature solution-processed carbonization and H_3PO_4 activation. *Bioresource Technology, 144*, 401–409.

Chiang, C. H., Chen, J., & Lin, J. H. (2020). Preparation of pore-size tunable activated carbon derived from waste coffee grounds for high adsorption capacities of organic dyes. *Journal of Environmental Chemical Engineering*, *8*, 103929.

Chu, G., Zhao, J., Huang, Y., Zhou, D., Liu, Y., Wu, M., Peng, H., Zhao, Q., Pan, B. & Steinberg, C. E. W. (2018). Phosphoric acid pretreatment enhances the specific surface areas of bio chars by generation of microspores. *Environmental Pollution*, *240*, 1–9.

Dehmani, Y., Franco, D. S., Georgin, J., Mghaiouini, R., Mohammed, B. B., Kacimi, R., Lamhasni, T., Lima, E. C., El Messaoudi. N., & Sadik, A. (2025). Towards a deeper understanding of the adsorption of methyl orange on a commercial activated carbon: Study of impact factors, isotherm and mechanism. *Environmental Surfaces and Interfaces*. *3*, 103–111.

Djilani, C., Zaghdoudi, R., Djazi, F., Bouchekima, B., Lallam, A., Modarressi, A., & Rogalski, M. (2015). Adsorption of dyes on activated carbon prepared from apricot stones and commercial activated carbon. *Journal of the Taiwan Institute of Chemical Engineers*, *53*, 112–121.

Fatama, K., Akter N., Saha, B., Nur-E-Alam, Md., & Chakma S. (2024). Minimization the chemical oxygen demand (COD) content in tannery wastewater using activated carbon from spent tea leaves. *Applied Environmental Research*, *46*(3), 036.

Fuentes, A. L. B., Barraqué, F., Mercader, R. C., Scian, A. N., & Montes, M. L. (2021). Efficient low-cost magnetic composite based on eucalyptus wood bio char for arsenic removal from groundwater. *Groundwater for Sustainable Development*, *14*, 100585.

Han, Q., Wang, J., Goodman, B. A., Xie, J., & Liu, Z. (2020). High adsorption of methylene blue by activated carbon prepared from phosphoric acid treated eucalyptus residue. *Powder Technology*, *366*, 239–248.

Ipeaiyeda, A. R., Choudhary, M. I., Ahmed, S. (2020). Ammonia and ammonium acetate aodifications and characterization of activated carbons from palm kernel shell and coconut shell. *Waste and Biomass Valorization*, *11*, 983–993.

Islam, M. A., Sabar, S., Benhouria, A., Khanday, W. A., Asif, M., & Hameed, B. H. (2017). Nanoporous activated carbon prepared from karanj *(Pongamia pinnata)* fruit hulls for methylene blue adsorption. *Journal of the Taiwan Institute of Chemical Engineers*, *74*, 96–104.

Jagtoyen, M., & Derbyshire, F. (1998). Activated carbons from yellow poplar and white oak by H_3PO_4 activation. *Carbon*, *36*(7), 1085–1097.

Kazmierczak-Razna, J., Nowicki, P., Wiśniewska, M., Nosal-Wiercińska, A., & Pietrzak, R. (2017). Thermal and physicochemical properties of phosphorus-containing activated carbons obtained from biomass. *Journal of the Taiwan Institute of Chemical Engineers*, *80*, 1006–1013.

Khamdahsag, P., Jarichanon, T., Phanthasri, J., Suwannatrai, S., Pangkumhang, B., & Tanboonchuy, V. (2021). Adsorption of dye over lignin obtained from wastewater separation, *Current Applied Science and Technology*, *21*(1), 165-175.

Kittappa, S., Jais, F. M., Ramalingam, M., Mohd, N.S., & Ibrahim, S. (2020). Functionalized magnetic mesoporous palm shell activated carbon for enhanced removal of azodyes. *Journal of Environmental Chemical Engineering*, *8*, 104081.

Kumar, N., Pandey, A., & Sharma, Y. C. (2023). A review on sustainable mesoporous activated carbon as adsorbent for efficient removal of hazardous dyes from industrial wastewater. *Journal of Water Process Engineering*. *54*,104054.

Luo, Y., Li, D., Chen, Y., Sun, X., Cao, Q., & Liu, X. (2019). The performance of phosphoric acid in the preparation of activated carbon-containing phosphorus species from rice husk residue. *Journal of Materials Science*, 54, 5008–5021.

Menya, E., Olupot, P. W., Storz, H., Lubwama, M., & Kiros, Y. (2018). Production and performance of activated carbon from rice husks for removal of natural organic matter from water: A review. *Chemical Engineering Research and Design*, *129*, 271–296.

Moghaddasi, F., Heravi, M. M., Bozorgmehr, M. R., Ardalan, P., & Ardalan, T. (2010). Kinetic and thermodynamic study on the removal of methyl orange from aqueous solution by adsorption onto camel thorn plant. *Asian Journal of Chemistry*, *22*, 5093–5100.

Mohamed, G. M., Rashwan, W. E. E., El-Nabarawy, T., & El-Hendawy, A. N. (2021). Removal of basic dyes from aqueous solution onto H_2SO_4-modified rice husk. *Egyptian Journal of Chemistry*, 64, 143–155.

Mohamed, F. M., Alfalos, A. M., Alrakshy, M. F., Aborziza, M. A., Alfalous, K. A., Rafea, M. A., Zaki, M. E., El-Aassar, M. R., & Roshdy, M. A. (2026). Sustainable removal of azo dyes from real effluents using a biomass-derived composite. *Scientific Reports*, *16*, 2076.

Ncibi, M. C., Ranguin, R., Pintor, M. J., Jeanne-Rose, V., Sillanpää, M., & Gaspard, S. (2014). Preparation and characterization of chemically activated carbons derived from Mediterranean Posidonia oceanica (L.) fibres. *Journal of Analytical and Applied Pyrolysis*, *109*, 205–214.

Pal, J., Deb, M., Deshmukh, D., & Verma, D. (2013). Removal of methyl orange by activated carbon modified by silver nanoparticles. *Applied Water Science*, *3*, 367–374.

Palapa, N. R., Taher, T., Juleanti, N., & Normah Lesbani N. A. (2021). Biochar from rice husk as efficient biosorbent for procion red removal from aqueous systems. *Applied Environmental Research*, *43*(3), 79–91.

Pasukphun N., & Suma Y. (2017). Preliminary study of color removal from Moh Hom dyeing wastewater using a low cost activated carbon derived from pineapple waste. *Applied Environmental Research*, *39*(3), 41–47.

Pereira, M. F. R., Soares, S. F., Órfão, J. J. M., & Figueiredo, J. L. (2003). Adsorption of dyes on activated carbons: influence of surface chemical groups. *Carbon*, *41*, 811–821.

Phothitontimongkol, T., & Prasertboonyai K. (2022). Process optimization and modeling of low-cost activated carbon preparation and its application in chromium (VI) removal. *Chiang Mai Journal of Science*, *49*(6), 1559–1575

Phothitontimongkol, T., & Prasertboonyai K. (2024). A fast removal of methyl orange from an aquatic system utilizing activated carbon from waste

tamarind wood. *Desalination and Water Treatment*, *317*, 100267

Pornsawai, P., Ngamsurach P., & Prasongdee, V. (2022). Comparative reactive blue 4 dye removal by lemon peel bead doping with iron(III) oxide-hydroxide and zinc oxide. *ACS Omega*, *7*, 41744–41758.

Rahmani, A. R., Asgari, G., Farrokhi, M., & Shirzad siboni, M. (2013). Removal of reactive black 5 (RB5) dye from aqueous solution using adsorption onto strongly basic anion exchange resin: Equilibrium and kinetic study, *Iranian Journal of Health and Environment*, 5(4), 509–518.

Rockwood, D. L., Ellis, M. F., Liu, R., Zhao, F., Ji, P., Zhu, Z., Fabbro, K. W., He, Z. & Cave, R.D. (2019). Short rotation eucalypts: Opportunities for biochar. *Forests*, 10(4), 314.

Saowanee, S., & Tangsathitkulchai, C. (2013). Adsorption of natural aluminium dye complex from silk-dyeing effluent using eucalyptus wood activated carbon. *American Journal of Analytical Chemistry*, *4*, 379–386.

Sawasdee, S., & Watcharabundit, P. (2024). Adsorption behavior and mechanism of brilliant green dye onto acid-modified mesoporous volcanic pumice. *Applied Environmental Research*, *46*(3), 042.

Singh, V., Soni, A., & Singh, R. K. (2016). Process optimization studies of malachite green dye adsorption onto eucalyptus (Eucalyptus globules) wood biochar using response surface methodology. *Oriental Journal of Chemistry*, *32*, 2621–2631.

Singh, B., Walia, B., & Arora, R. (2018). Parametric & kinetic study for the adsorption of crystal violet dye by using carbonized eucalyptus. *International Journal of Computational Engineering Research*, *8*, 1–11.

Singh, B., Walia, B. S., & Arora, R. (2023). Adsorption performance of eucalyptus bio char fixed-bed column for manganese removal in actual groundwater. *Journal of Science and Technology Mahasarakham University*, *42*, 178–186.

Suma, Y., Pasukphun, N., & Eaktasang N. (2021). Adsorption of methylene blue by low-cost biochar derived from elephant dung. *Applied Environmental Research*, *43*(3), 34–44.

Sych, N. V., Trofymenko, S. I., Poddubnaya, O. I., Tsyba, M. M., Sapsay, V. I., Klymchuk, D. O., & Puziy, A. M. (2012). Porous structure and surface chemistry of phosphoric acid activated carbon from corncob. *Applied Surface Science*, *261*, 75–82.

Zein, R., Akmal, C., Safni, S.,Fauzia, S., & Ramadhani, P. (2023). Banana stem *(Musa balbisiana Colla)* as potential biosorbent to remove methylene blue dye in wastewater: isotherm, kinetic, thermodynamic studies and its application. *Applied Environmental Research*, *45*(3), 015.